An update of dynamic thermal-hydraulic simulations of the JT-60SA Toroidal Field coil cooling loop for preparing plasma operation

S. Varin, F. Bonne, C. Hoa, S. Nicollet, L. Zani, J.-C. Vallet, K. Fukui, K. Natsume

Version of Record: https://www.sciencedirect.com/science/article/pii/S0011227520300941
Manuscript_75229e882ff8010df452b12085ee3fca

CHATS on Applied Superconductivity 2019

An update of dynamic thermal-hydraulic simulations of the JT-60SA Toroidal Field coil cooling loop for preparing plasma operation

S. Varin[a], F. Bonne[a], C. Hoa[a], S. Nicollet[b], L. Zani[b], J-C Vallet[b], K. Fukui[d], K. Natsume[d]*

[a]*Univ. Grenoble Alpes, CEA IRIG-DSBT, Grenoble, 38000, France*
[b]*CEA/IRFM Saint-Paul-lez-Durance 13108 France*
[d]*Naka Fusion Institute, National Institute for Quantum Radiological Science and Technology, 801-1 Mukoyama, Naka, Ibaraki, 311-0193 Japan4*

ARTICLE INFO

Article history:
Received 00 December 00
Received in revised form 00 January 00
Accepted 00 February 00

Keywords:
Fusion
Superconducting magnets
Pulsed loads
Cryo-distribution
Supercritical helium

ABSTRACT

The JT-60SA cryogenic system was commissioned in 2016 in closed loop, without the cryogenic users (superconducting magnets, current leads, thermal shields). The first plasma operation is expected in 2020. This paper updates the heat load profiles resulting from the cooling loop of TF magnets, and received by the refrigerator and its thermal damper. The heat load profiles are calculated through thermal-hydraulic simulations of the magnets and the associated cryo-distribution, also named as supercritical helium loops. This update was performed by taking into account new data from the TF magnets (measured pressure drops, updated heat loads coming from the plasma), as well as a more accurate thermal model of the TF magnet. Previous simulation had been performed using the Vincenta code in 2010 and were used for the cryogenic system acceptance tests. The new thermal-hydraulic model is performed by using Simcryogenics, the modeling tool dedicated to refrigeration and cryo-distribution developed by CEA (Commissariat à l'énergie atomique et aux énergies alternatives). The differences between the two simulation results are highlighted and analyzed. These simulations provide the pulsed heat load profiles smoothed by the cryo-distribution and deposited into the thermal damper.

1. Introduction

In the framework of the Broader Approach, the joint European Japanese superconducting tokamak, JT-60SA, will be commissioned in 2020 in Naka, Japan [18]. The motivation of this work is to have an updated thermal hydraulic modelling of the cryogenic loop supplying the TF coils and coil structures and the associated cryo-distribution to be used for the preparation of the future operation of the tokamak.

The cryogenic system has been commissioned in 2016 [17], using by-pass lines and heaters to simulate the pulsed heat loads from the cryogenic users. Among the cryogenic users, the superconducting magnets are cooled by two supercritical helium loops at 4.4 K and 5 bar. Loop 1 is dedicated to the Toroidal Field coils (TF) and the cold structures while loop 2 supplies the Central Solenoid (CS) and Equilibrium Field coils (EF). In addition to these two loops, there are a loop 3 supplying the cryopumps at 3.7 K, a loop 4 supplying the thermal shields at 80 K and a loop 5 supplying HTS current leads at 50 K. The performance of the cryogenic system was demonstrated during the acceptance tests by showing that the system could extract the pulsed heat loads due to cycling plasma operation [16].

At the time of the specification of the cryogenic system, the pulsed load profiles for the acceptance tests were derived from dynamic thermal-hydraulic modelling using Vincenta [5]. Several codes have been used to model TF magnets such as 4C [19] and THEA [20], in particular for quench studies. Simcryogenics has been developed by CEA for quick dynamic simulations for control with model-based design [25] and for design optimization through parametric studies [12]. The reliability and optimization of operation become challenging aspects to study with quick dynamic simulations. It requires simplified models for faster-than-real time calculations. Some methodologies have been developed and tested, for example for ITER TF and CS magnets based on Artificial Neural Network requiring training of the neural network on full sets of simulations with detailed models [26]. Simcryogenics developed by CEA for the cryo-distribution and the cryoplant is addressing the critical requirement of dynamic simulations for control purposes with simplified models**.**

Recent modelling work with Simcryogenics demonstrated the relevance of the thermal-hydraulic code developed by CEA for modelling the cryo-distribution and the cable in conduit conductors (CICC), in order to evaluate the heat load profile to the cryoplant [7]. This work, as well as the present one, is focusing on the supercritical helium loop of the Toroidal Field coils and the structures (loop 1). The present work is an update of the previous modelling, taking into account all the latest information on the TF superconducting coils following manufacturing and the testing in the Cold Test Facility [1] under cryogenic conditions. Indeed, the available measurements on the 18 TF coils could provide updated friction factor correlations [2]. The model assumptions were detailed and revised with more refined heat load distributions on the TF CICC. These assumptions were also revised in terms of dimensions and

* *Corresponding author.*
E-mail address: christine.hoa@cea.fr

materials of the CICC as well as correlations for the convective heat transfer coefficient in the CICC and cryo-distribution pipes. The thermal hydraulic model of the conductors is also improved by taking into account the inter-turn thermal coupling of the pancake-wound conductors. The effect of the inter-turn thermal coupling has been previously studied for TF quench modelling, within the framework of various fusion projects, *e.g.* JT-60 SA [21], ITER [22] and DEMO [23]. The thermal coupling was found to be a relevant phenomenon to model.

The impact of these different improvements are highlighted and discussed. The updated profile of the heat load deposited in the thermal damper is presented.

Nomenclature

Nu Nusselt number, -
Re Reynolds number, -
Pr Prandtl number, -
f_D Darcy friction factor, -
V_f Void fraction, -
ΔP Pressure drop across the TF CICC, Pa
L Length of the TF CICC, m
D_h Hydraulic diameter of the TF CICC, m
ρ Density of helium flowing through the TF CICC, kg/m^3
V Velocity of helium flowing through the TF CICC, m^2/s
R_{it} Thermal resistance for the inter-turn thermal coupling, m^2.K/W
e_{SS} Thickness of stainless steel of the jacket, m
e_{GE} Thickness of glass-epoxy insulation, m
λ_{SS} Thermal conductivity of stainless steel, W/(m.K)
λ_{GE} Thermal conductivity of glass-epoxy, W/(m.K)
$P\ circ$ Pressure of the circulating pump, bar
T_{TF} Temperature of TF CICC, K
$T_{TF\ str}$ Temperature of TF structures, K
$T_{CS\ str}$ Temperature of CS structures, K
$\dot{m}_{TF}$ Mass flowrate through TF CICC, kg/s
Q_{HX2} Power received by the heat exchanger HX2 and deposited into the thermal damper V700, W

2. Description of loop 1 & TF CICC

The TF & Structures loop, also called loop1, uses supercritical helium to cool the 18 Toroidal field (TF) coils and their structures, i.e. TF structures (TF STR), as well as CS structures (CS STR), as shown in Fig. 1. One TF coil consists of a winding pack made of 6 Double-Pancakes (WP) supported by a stainless steel casing. Each Double-Pancake is made of a Cable-In-Conduit Conductor (CICC), whose characteristics are listed in Table 1.

Table 1- Characteristics of the TF CICC

Properties	
Length (m)	113
Void fraction (-)	0.32
Strand diameter (mm)	0.81
Number of superconducting strands	324
Number of copper strands	162

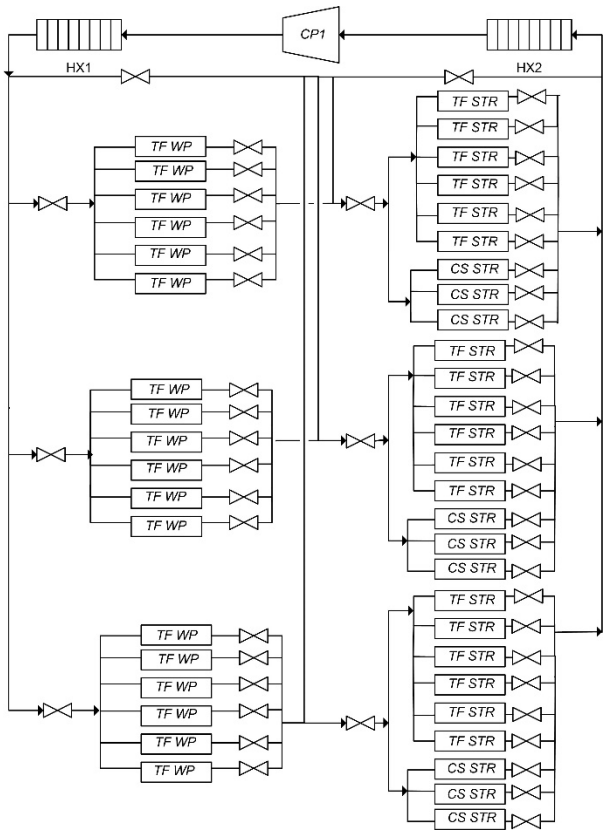

Fig. 1 – Simplified Process Flow Diagram of loop 1

3. Model description

3.1. Description of the Vincenta model

A model of the loop 1 was performed using the Vincenta code V6.0 in 2010 [5]. The Vincenta code is a thermal-hydraulic simulation code for superconducting magnets and their cryo-distribution. This code was used to model the dynamic behavior of the supercritical loop HELIOS (Helium Loop for hIgh LOads Smoothing) under pulsed heat loads [6]. Since the comparison to experimental results gave very satisfying results [6], the Vincenta code was chosen to benchmark the model of the loop 1 performed using the Simcryogenics library [7]. The results obtained using Vincenta in 2010 are considered in the present paper. Since 2010, CEA/dSBT has developed its own modelling tool Simcryogenics, which was chosen for the present modelling work. This tool is more flexible allowing the reduction of the calculation time (typically 10 min for the loop), the study of various dynamic scenarios including the refrigerator (e.g. pulsed heat load scenarios, cool-down scenarios) as well as the analysis of control strategies.

3.2. Description of the Simcryogenics models

The loop1 was modelled using the Simcryogenics library for MATLAB/Simulink, as schematically shown in **Fig. 2**. 1-dimensional pipes, *i.e.* pipes consisting of volumes distributed along the flow direction, were used to model the supply line, return line, TF CICC as well as TF and CS structures. The two exchangers HX1 and HX2 were considered as

perfect heat exchangers, *i.e.* the outlet temperature was independent of flow conditions and set equal to the bath temperature. These exchangers were immersed into the thermal damper V700, which is a 4.3 K saturated helium bath. The schematic is similar to that presented in [7] even though the library had been updated in order to manage flow reversal [12]. Equivalent parallel channels were only modelled once and then multiplied. Similarly, only one pancake of the TF coil was modelled, as shown in **Fig. 3**. As the heat load and the pressure drop differ from one pancake to another, a mean friction factor and heat load were applied on the modelled pancake. The modelled pancake was considered a central pancake and the 2-dimensionnal effects of the cooling channels in the casing were therefore neglected. Central pancakes are the most constraining pancake based on the distribution of magnetic fields [24] [23]. **Fig. 4** shows the schematic that was used to model the TF & CS structures. One fluid channel is modelled for TF structures and CS structures by a 1-dimensional pipe and a 1-dimensionnal mass. This is a simplified model of the structures where the delay time due to the heat propagation through the cooling pipes as well as the thermal coupling between the TF winding pack and its structure are not considered. Comparisons that have been performed with and without the modelling of the structure on DEMO TF coil with THEA [24] have shown that the differences in terms of temperature margin remain small. Moreover, neglecting the cooling of the structure is a conservative approach concerning the evaluation of the heat load profile to the cryoplant.

The purpose of this simplified model of loop 1 is to have an estimate of the heat load arriving at the refrigerator. This model is not accurate enough to provide either refined thermal-hydraulic simulation (temperature margin) or the analysis of an accidental scenario (quench), but can be used to study operating scenarios, such as pulsed heat loads, and the analysis of control strategies.

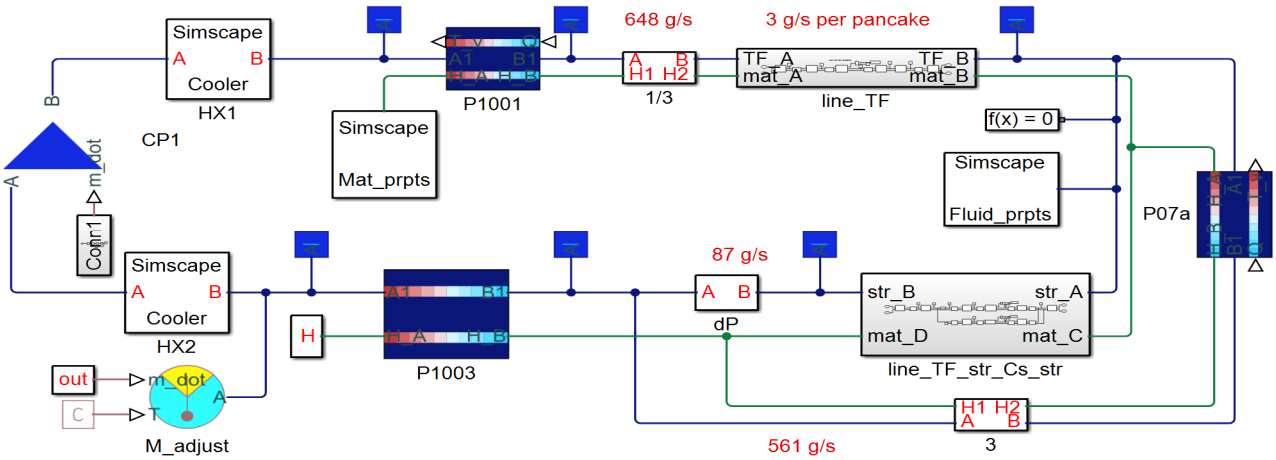

Fig. 2 - Schematic of the Simcryogenics models, which include the heat exchangers HX1 and HX2, cryo-distribution pipes (P1001, P1003, P07a), the circulating pump CP01 as well as the lines detailed in Fig. 3 and Fig. 4. The blue connections are fluid connections while the green ones convey materials properties. The mass flowrates are indicated for a reduced mass flowrate of 3 g/s. The mass flowrate flowing through the structures can be adjusted via by-pass valves, which are not shown in the present figure. The purpose of the element M_adjust is explained in section 4.1.

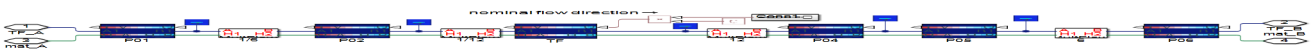

Fig. 3 - Schematic of the line_TF subsystem, which contains the TF CICC referred to as TF. A heat load is applied on TF according to section 4.5. The elements P01 to P06 are cryo-distribution pipes. The flow multiplication performed by the elements 1/6, 1/12, 12, 6 results from the number of TF coils and channels per TF coil, respectively 18 and 12.

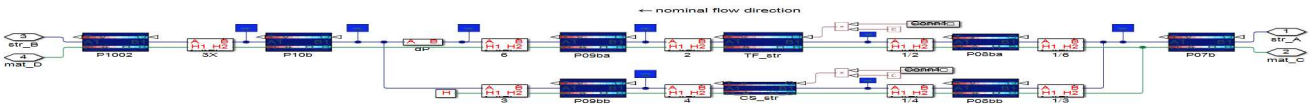

Fig. 4 - Schematic of the line_TF_str_Cs_str subsystem, which contains the TF & CS structures referred to as TF_str & CS_str. The elements P07b to P1002 are cryo-distribution pipes. Flow multipliers are used in order to consider the total number of helium circuits inside the TF and CS structures.

Two distinct models were developed on Simcryogenics. The first one aimed at reproducing the results that were obtained using the Vincenta code. This Simcryogenics model was built using the data that were available in 2010 and will be referred to as SC1 model in the following sections. The second one was an updated SC1 model, which was dedicated to the study of the different modifications in terms of heat transfer coefficient, friction factor, materials properties and non-uniformly distributed heat load distribution on the TF CICC. This model was also modified in order to model the inter-turn thermal coupling, as defined in section 4.6. In the following sections, the updated model will be referred to as SC2 model.

4. Model assumptions

4.1. Initial conditions

On Vincenta and Simcryogenics models, the loop is considered isochoric. In order to be able to compare Simcryogenics results to those obtained with Vincenta, the initial mass of helium was adapted on Simcryogenics so that the initial inlet pressure of the loop was similar to that of Vincenta. This was performed by using a charge or discharge charge valve at the beginning of simulation, modelled by a mass flowrate source or sink, as shown in **Fig. 2**. Once this adjustment has been performed, the loop is isochoric.

4.2. Correlation for convective heat transfer

Constant values were used for convective heat transfer coefficients for both Vincenta and SC1 model. The convective heat transfer coefficient between the helium flowing through the CICC and the CICC material was 25 W/(m^2.K), while a value of 750 W/(m^2.K) was chosen for the heat transfer coefficient between the helium and the TF & CS structures. Heat transfer coefficients were calculated on SC2 model using the Dittus-Boelter correlation, as follows:

$$Nu = 0.023 \times Re^{0.8} \times Pr^{0.4} \quad (1)$$

JT60-SA TF CICC have also been modelled in previous work using the Dittus-Boelter-Giarratano correlation [4] and the Colburn-Reynolds analogy [13], based on the model and tests that were performed for ITER CICC [14]. The Colburn-Reynolds analogy can be written as follows:

$$Nu = \mathrm{f_D}/8 \times Re \times Pr^{1/3} \quad (2)$$

Typical values of heat transfer coefficient inside the CICC at 3g/s are respectively about 5.4×10^2 and 3.1×10^3 W/(m^2.K) for the Dittus-Boelter correlation and Colburn-Reynolds analogy. For both methods, the temperature difference between the mass of materials and the fluid is only a few mK, due to the high values of heat transfer coefficient and heat transfer area. Therefore, the choice between Eq. 1 and Eq. 2 have a negligible impact on the results, as shown in section 5.6.

4.3. Friction factor

The pressure drop was calculated by using the Darcy-Weisbach equation as detailed in Eq. 3. The Darcy friction factors of pipes, TF CICC and TF & CS structures were calculated accordingly for the different models.

$$\Delta P = f_D \times \mathrm{L/D_h} \times \rho \times \mathrm{V^2}/2 \quad (3)$$

The Darcy friction factors of distribution pipes and TF & CS structures were calculated by using Altshul formula [10] for the Vincenta and Simcryogenics models:

$$f_D = 0.11 \times (68/Re + Rr)^{0.25} \quad (4)$$

On Vincenta and SC1 models, the friction factor of TF CICC was calculated using a modified Katheder correlation [8], which was proposed by Nicollet et al.[3][2][9]:

$$f_D = (19.5/\mathrm{Re}^{0.7953} + 0.0231)/V_\mathrm{f}^{0.742} \quad (5)$$

With a void fraction V_f of 0.32

Since 2010, new data regarding the friction factor of TF CICC have become available. Decool et al. conducted a characterization program of TF CICC and the measurement of their friction factor [2]. The pressure drop inside the TF coils was found to be higher than expected. A new correlation for the friction factor was therefore determined with specific coefficients, *i.e.* α, β, and γ, for each double-pancakes of each TF coil [2]:

$$f_D = \alpha + \beta \times Re^{\gamma} \quad (6)$$

Only one pancake is modelled on Simcryogenics as all pancakes are considered equivalent. In order to update the friction factor on SC2 model, Eq. 6 was used after averaging the experimental coefficients that were measured for each double-pancakes of the TF coil 12 [4].

$$f_D = 0.101 + 35.7 \times Re^{-0.729} \quad (7)$$

In order to maintain a pressure drop inside the TF CICC of 1.1 bar despite these higher values of the friction factor, a reduced value of 3 g/s was

chosen for the mass flowrate flowing through the TF CICC instead of the previous value of 4 g/s [7].

4.4. Dimensions & materials for the TF CICC

The parameters used to model the TF CICC are shown in Table 2. On SC2 model, the wetted perimeter, the helium cross-section area as well as the type and masses of materials were updated according to [4]. As for the modified SC2 model dedicated to the study of the inter-turn thermal coupling, the bundle and the jacket with its insulation were modelled as two distinct masses, as described in section 4.6. On Simcryogenics, the material properties of copper, stainless steel and epoxy were calculated using data from NIST. An updated value of 100 was chosen for the RRR of copper based on the measurement that were performed on the CICC copper and NbTi strands, *i.e.* ranges of 70-90 and 148-233 respectively [15].

4.5. Heat loads

After the Vincenta model of 2010 was established, a contingency of about 14% has been added to the heat load on the TF CICC, TF & CS structures as well as TF joints. The updated load of the latter is 315 W, while the updated dynamic load profiles are shown in Fig. 5 and Table 3. Static losses of about 200 W were added to represent the cryo-distribution losses in the Simcryogenics models and the Vincenta model.

Table 2- Data used for the TF CICC on the different models

	Vincenta & SC1 model	SC2 model
Length (m)	113	113
Void fraction (-)	0.32	0.32
Wetted perimeter (m)	1.111	1.108
Helium cross-section area (m^2)	1.27e-4	1.25824e-4
Masses of materials for one pancake	425 kg of copper (RRR=300)	157 kg of 316 stainless steel, 182 kg of copper (RRR=100) and 42 kg of NbTi

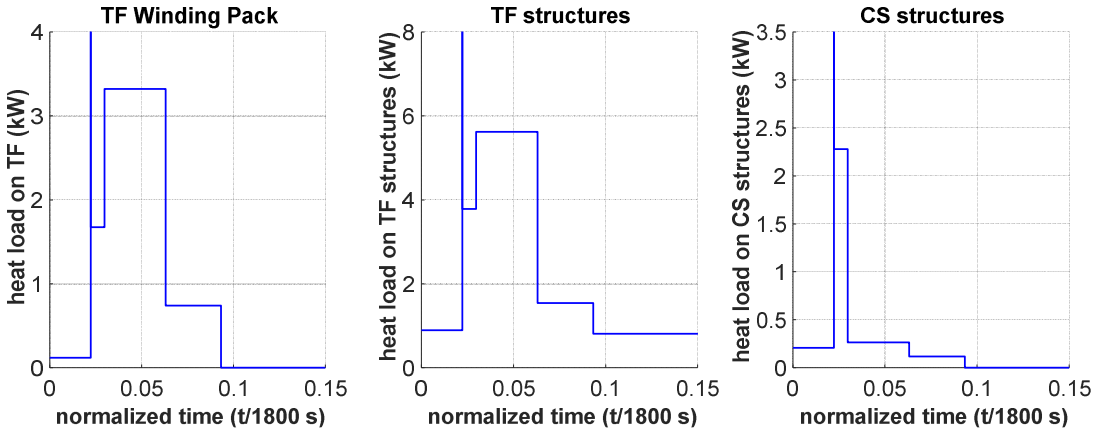

Fig. 5 – Overall updated heat load profiles for TF Winding Pack, TF structures and CS structures as a function of normalized time (normalized in relation to the cycle time of 1800 s). For the TF and CS structures, the y-axis has been truncated as a peak of respectively 266.1 kW and 122.6 kW can be noted during plasma initialization

Table 3- Overall updated heat load profiles for TF Winding Pack (TF WP), TF structures and CS structures

Duration (s)	Heat load on TF WP (kW)	Heat load on TF WP (kJ)	Heat load on TF structures (kW)	Heat load on TF structures (kJ)	Heat load on CS structures (kW)	Heat load on CS structures (kJ)
40	1.21E-01	4.82E+00	8.95E-01	3.58E+01	2.08E-01	8.31E+00
0.15	4.93E+00	7.39E-01	2.66E+02	3.99E+01	1.23E+02	1.84E+01
13.4	1.67E+00	2.24E+01	3.78E+00	5.06E+01	2.28E+00	3.05E+01
60	3.32E+00	1.99E+02	5.62E+00	3.37E+02	2.65E-01	1.59E+01
54.3	7.41E-01	4.02E+01	1.54E+00	8.38E+01	1.17E-01	6.38E+00
1632.15	0.00E+00	0.00E+00	8.10E-01	1.32E+03	0.00E+00	0.00E+00

4.6. Inter-turn thermal coupling

The TF CICC is a cable made of NbTi and Cu strands inside a stainless steel jacket, which is insulated against the other conductors using epoxy, as shown in Fig. 7. The CICC in one pancake is wound in 6 turns. The inter-turn thermal coupling is the thermal coupling occurring between the successive turns of the jacket that are in contact.

SC2 model was modified in order to investigate the effect of the inter-turn thermal coupling. The CICC was therefore divided between 3 elements: the jacket, the bundle and the fluid channel, as shown in Fig. 6. The thermal coupling was modelled by connecting the different meshed elements of the jacket that were in contact thermally via thermal resistances. The thermal resistance was calculated as follows:

$$R_{it} = 2 \times \mathrm{e_{SS}}/\lambda_{\mathrm{SS}} + e_{GE}/\lambda_{\mathrm{GE}} \quad (6)$$

With a thickness of stainless steel e_{SS} and glass-epoxy e_{GE} of 2 mm.

The thermal conductivity of stainless steel and epoxy was calculated as a function of temperature during simulation for each element of the meshed 1D mass of materials. The thermal conductance associated with inter-turn thermal coupling per meter of CICC ranged from 0.69 to 0.72 W/(m.K) for the simulation described in section 5.5.2. The pancake-to-pancake thermal coupling was not considered in the present study, but would constitute a further improvement of the model.

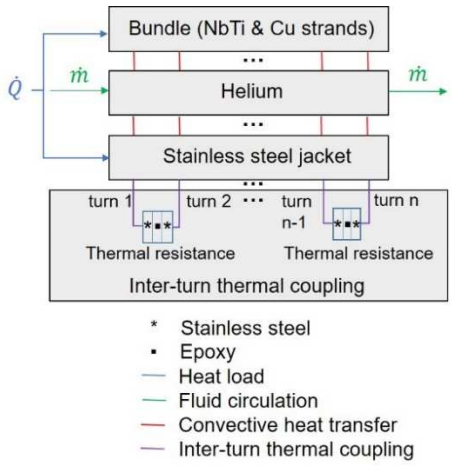

Fig. 6 - Schematic used to model the inter-turn thermal coupling

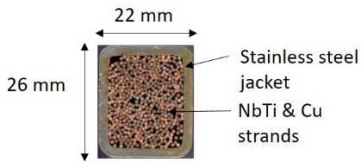

Fig. 7 – Cross-section of the CICC (Courtesy of F4E)

The heat load received by the TF winding pack was distributed along the different turns by applying the distribution profile described in Table 4. This profile is a rough estimate that was extrapolated from DEMO calculations [11]. A non-uniformly distributed profile was chosen instead of a uniform one, as this profile is more realistic while being more critical. This allows the smoothing effect of the inter-turn thermal coupling to be illustrated. This heat load was then distributed between the jacket and bundle according to their respective mass ratios.

Table 4- Non-uniformly distributed heat load distribution on TF CICC

	Heat load distribution
Turn 1	51 %
Turn 2	21 %
Turn 3	13 %
Turn 4	7 %
Turn 5	4 %
Turn 6	4 %

5. Results and discussion

5.1. Benchmark of Simcryogenics and Vincenta results

Under similar assumptions, the Vincenta code and the Simcryogenics library give similar results [7]. As an update of the Simcryogenics library was performed [12], it was necessary to verify that the results obtained with SC1 model were similar to those obtained with the Vincenta code using the same input parameters. As shown in Fig. 8, both results were in good agreement. For the different curves, the maximum absolute relative difference ranged from 0.6% to 7.5%, while the mean absolute relative difference ranged from 0.1% to 2.3%.

5.2. Update of heat loads & heat transfer coefficient

The heat loads were updated as described in section 4.5 on SC2 model, taking into account a 14% contingency. The materials and the dimensions of the CICC were also updated as detailed in section 4.4. The results obtained using SC1 model and SC2 model were compared. As shown in Fig. 9, this update resulted in an increase in temperature for TF & CS structures as well as an increase of the power received by the heat exchanger HX2. An increase in temperature of 0.17 and 0.12 K was respectively observed for the maximum outlet temperature of TF & CS structures. The maximum power received by the heat exchanger HX2 was found to be about 2.8 kW. This power is the power deposited into the thermal damper V700 of the refrigerator. No significant increase in temperature was observed inside the TF CICC.

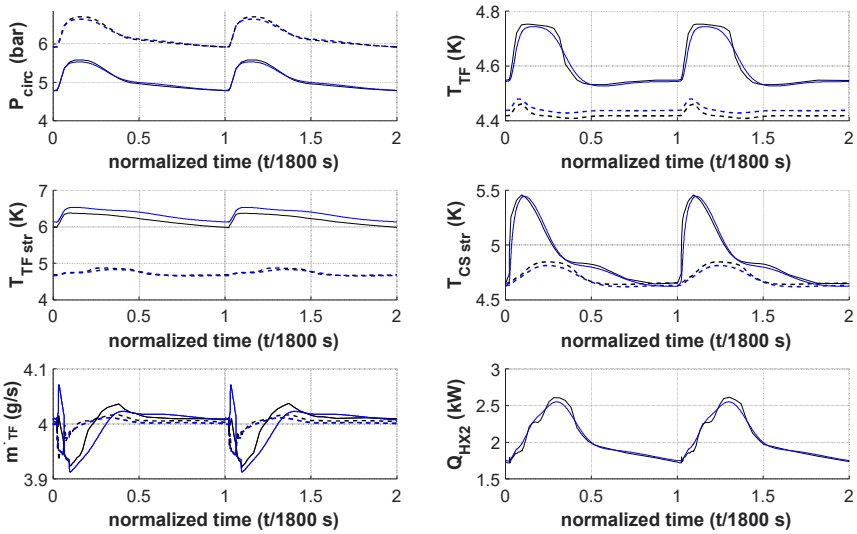

Fig. 8 - Comparison between the results obtained using Vincenta (black curve) and SC1 models (blue curve). Dashed lines and solid lines respectively show the inlet and outlet values.

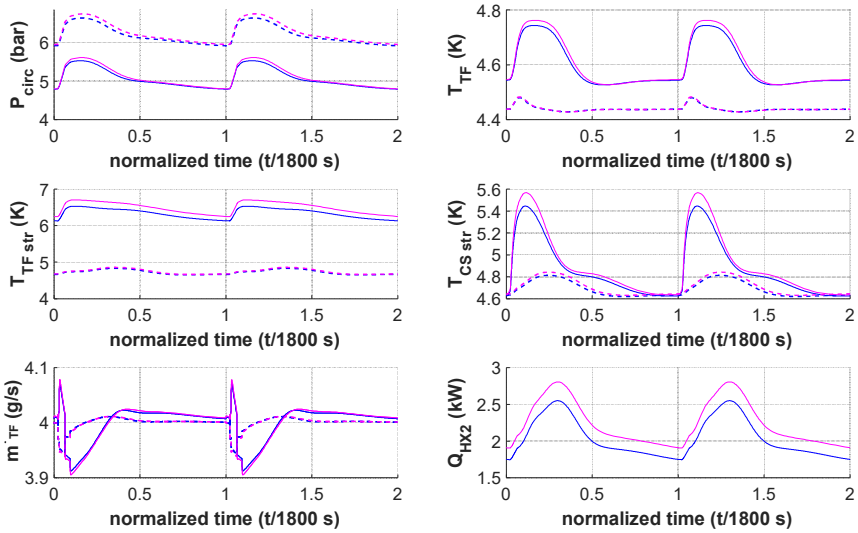

Fig. 9 - Comparison between the results obtained using SC1 (blue curve) and SC2 model after the update regarding the heat loads and the heat transfer coefficient as described in section 5.2 (magenta curve). Dashed lines and solid lines respectively show the inlet and outlet values.

5.3. Update of friction factor and reduced mass flow of 3g/s

The previous results obtained in section 5.2 with SC2 model were modified by reducing the nominal mass flowrate to 3 g/s and using Eq.(7) in order to calculate the Darcy friction factor. **Fig. 10** shows the obtained results. The use of a reduced mass flowrate of 3 g/s, due to the higher-than-expected pressure drop, resulted in an increase of the temperatures of the structures, but did not have a significant impact on the maximum TF CICC inlet or outlet temperature. This can be explained by the high values of heat transfer coefficient for TF CICC at 3 g/s and 4 g/s. Nevertheless, the TF CICC outlet temperature reached its initial value at the end of one heat load pulse after a longer duration.

A decrease in the heat load received by the heat exchanger HX2 as well as a smoother heat load profile was observed. The peak heat load received by HX2 was reduced from 2.8 to 2.4 kW. The specific enthalpy of the fluid at the inlet of HX2 was similar in both cases due to the same expansion in the loop and therefore the same increase in temperature resulting from the

Joule-Thomson effect. The temperature of the fluid at the outlet of HX2 was set by the temperature of the bath. Hence, a similar variation of specific enthalpy was observed in both cases between the inlet and outlet of HX2. The reduction of peak heat load was therefore caused by the reduction of mass flowrate. These results are consistent with those previously obtained by Bonne et al. [7], even though the latter were obtained under assumptions that differed from the present model, *e.g.* different values of heat load, heat transfer coefficient and friction factor

5.4. Non-uniformly distributed heat load profile

The SC2 model presented in section 5.3. was then updated by assuming a non-uniformly distributed heat load profile along the TF CICC. This profile was estimated from DEMO calculation [11] and detailed in section 4.6. This simulation aimed at investigating the effect of a non-uniformly distributed heat load profile and highlighting the influence of the inter-turn thermal coupling that is studied in section 5.5. As shown in **Fig. 11**, a non-uniformly distributed heat load profile resulted in an increase of the maximum TF outlet temperature and the maximum power received by the heat exchanger HX2. The assumption of a non-uniformly distributed profile is therefore conservative. A time shift was observed for the maximum values of the TF outlet temperature and HX2 power. This resulted from the reduced mass flow rate and the impact of the non-uniformly distributed heat load on the heat transport along the CICC.

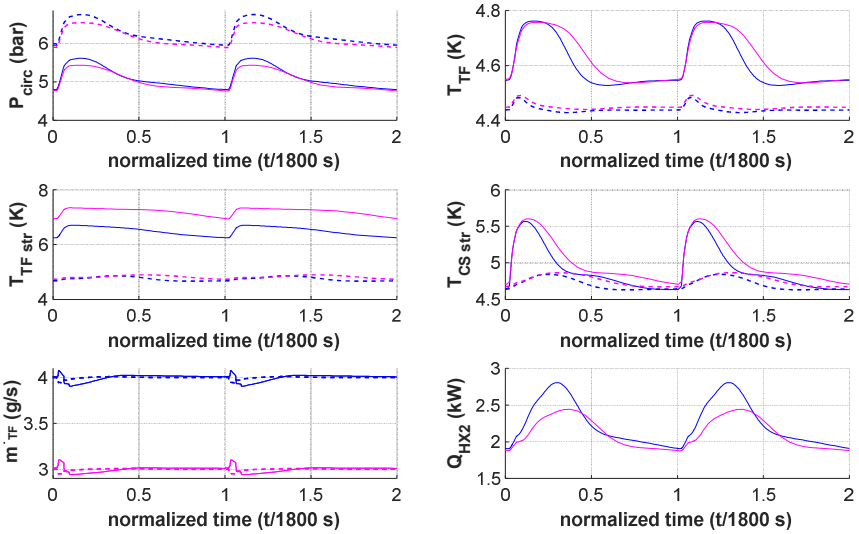

Fig. 10 - Comparison between the results obtained using SC2 model after the update regarding the friction factor as described in section 5.3 (magenta curve) and those obtained before the update (blue curve). Dashed lines and solid lines respectively show the inlet and outlet values.

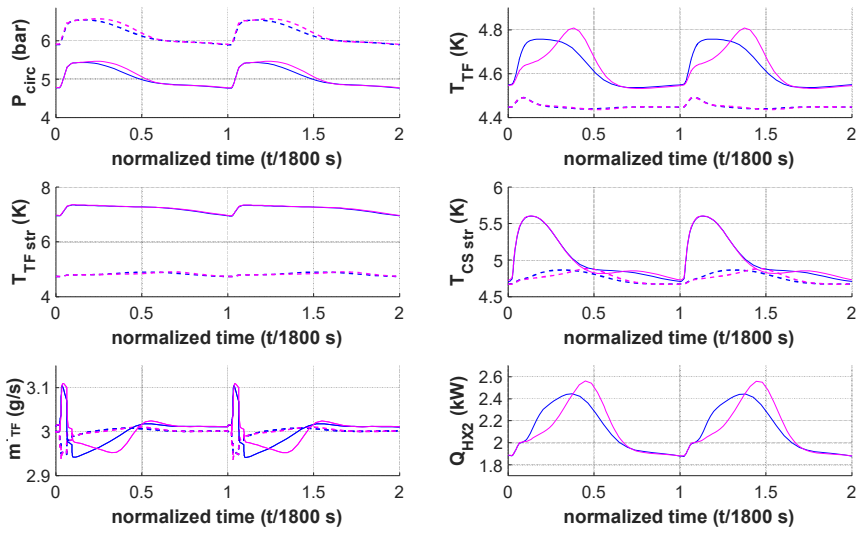

Fig. 11 - Comparison between the results obtained using SC2 model after the update regarding the non-uniformly distributed heat load as described in section 5.4 (magenta curve) and those obtained before the update (blue curve). Dashed lines and solid lines respectively show the inlet and outlet values.

.

5.5. Inter-turn thermal coupling

5.5.1. Comparison between simulation and experimental measurement

TF coils were tested in the Cold Test Facility, whose experimental setup was described by Abdel Maksoud et al. [1]. In order to study the heat propagation along the CICC and the effect of the thermal inter-turn coupling, an additional test was performed in this facility. This test consisted in testing one TF coil for a fast increase of the inlet temperature of about 1 K and observing the evolution of the outlet temperature.
A model of the experiment was built by using the TF CICC of SC2 model. The measured profile of inlet pressure, inlet temperature and outlet pressure were set as boundary conditions. Simulations were performed with and without taking into account the inter-turn thermal coupling. The simulated outlet temperature profile was compared to the experimental profile, as shown in **Fig. 12**. The model with inter-turn thermal coupling was found to be more consistent with the experimental results, thus showing the importance of modelling this phenomenon and validating the calculation of the inter-turn thermal coupling resistance.

5.5.2. Update of Simcryogenics results with inter-turn thermal coupling

The results presented in section 5.4 were updated by modelling the inter-turn thermal coupling, as shown in **Fig. 13**. The maximum TF outlet temperature and the maximum power received by the heat exchanger HX2 were reduced by respectively 73 mK and 0.15 kW. The inter-turn thermal coupling was therefore found to have a smoothing effect on the non-uniformly distributed heat load. However, a longer duration was required for the TF CICC outlet temperature to reach its initial value at the end of one heat load pulse.

5.6. Comparison between Dittus-Boelter correlation and Colburn-Reynolds analogy

As mentioned in section 4.2, some simulations were also performed by using the Colburn-Reynolds analogy in order to calculate the heat transfer coefficient. The updated SC2 model of section 5.5.2 was run with both the Colburn-Reynolds analogy and the Dittus-Boelter correlation. **Fig. 14** shows the obtained results. It can be noted that similar results were obtained, except for the outlet temperature of CS structures for which a higher value was obtained by using the Colburn-Reynolds analogy. An increase of 33 mK was observed for the maximum outlet temperature of the TF CICC. This resulted from higher values of heat transfer coefficient when using the Colburn-Reynolds analogy. As little difference was observed between the two correlations, the results obtained using Dittus-Boelter correlation in section 5.5.2. will be the baseline for future analyses.

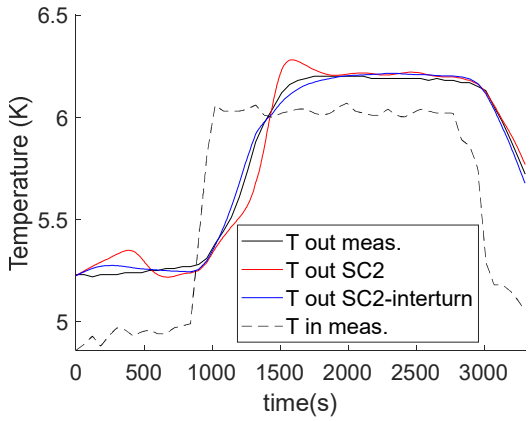

Fig. 12 –Comparison between measured TF inlet & outlet temperature profiles (black curves) and Simcryogenics results using SC2 model with inter-turn thermal coupling (blue curve) and without inter-turn thermal coupling (red curve).

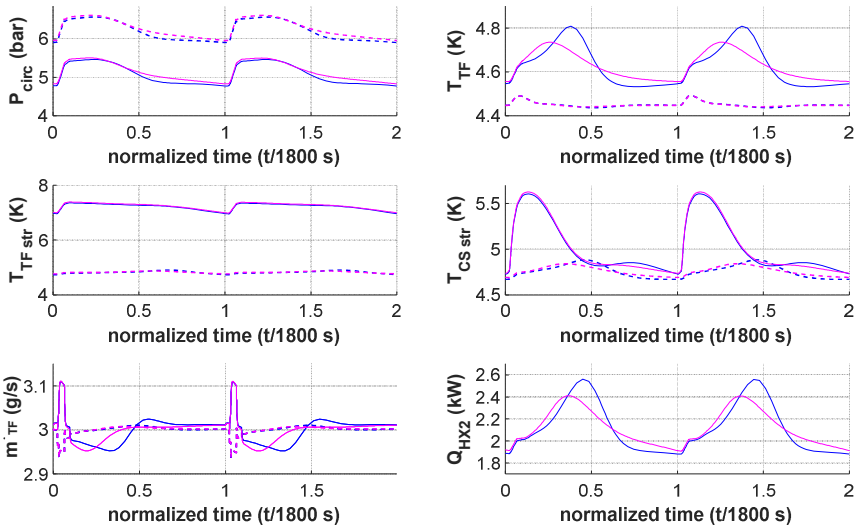

Fig. 13 - Comparison between the results obtained using SC2 model after the update regarding the inter-turn thermal coupling as described in section 5.5 (magenta curve) and those obtained before the update (blue curve). Dashed lines and solid lines respectively show the inlet and outlet values.

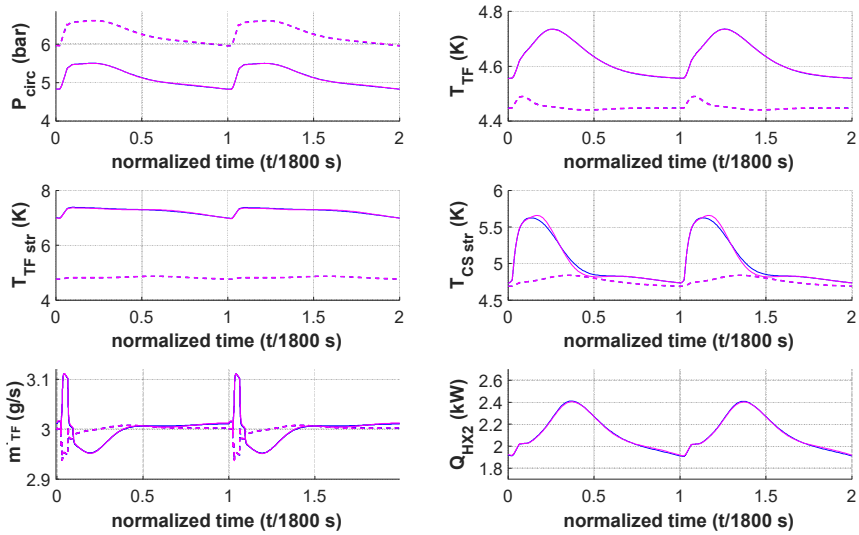

Fig. 14 - Comparison between the results obtained using SC2 model with Dittus-Boelter correlation (blue curve) and Colburn-Reynolds analogy (magenta curve). Dashed lines and solid lines respectively show the inlet and outlet values.

6. Conclusion

A model of the TF & Structures loop (loop 1) was developed using Simcryogenics in order to reproduce the simulations that were performed in 2010 by using the Vincenta code. This previous model, which aimed at determining the pulsed heat load profile, had been used to specify the dynamic refrigeration operation of the JT-60SA cryogenic system.

An updated model was built in order to take into account the latest information related to the manufacturing and testing of TF coils. The most significant changes of the model were the consideration of the 14% contingency for the heat load, the update of the friction factor, the reduced

mass flowrate, the non-uniformly distributed heat load on the TF CICC and the inter-turn thermal coupling of the TF CICC.

The effect of the inter-turn thermal coupling was found to counterbalance the effect of the non-uniformly distributed heat load. The difference between the updated profile of the heat load deposited in the thermal damper and that obtained in 2010 was therefore mainly due to the update of the heat load and the use of a reduced mass flowrate along with an updated friction factor. The updated profile of the heat load deposited in the thermal damper was found to be smoother than that obtained in 2010.

The modelling work performed using Simcryogenics can be used for preparing the plasma operation of JT-60SA in the coming years. In the future, perfect heat exchangers would be modified in order to model a finite-sized bath and therefore the temperature variation of the bath and hence the variation of the inlet temperature. Similar updates will be performed to simulate CS & EF coils loop (loop 2) in the future. The model can be coupled with the cryogenic system model and can be used for testing the control strategies related to pulse operation as well as investigating cool down scenarios.

Acknowledgements

The authors would like to thank the CTF team for the tests ATA02 and the data regarding coils, in particular Roser Vallcorba for providing the data. The authors would like to thank Manfred Wanner for his advices and fruitful discussions regarding the interpretations of the present results.

This work was undertaken under the Broader Approach Agreement between the European Atomic Energy Community and the Government of Japan. The views and opinions expressed herein do not necessarily state or reflect those of the Parties to this Agreement.

References

[1] Abdel Maksoud, W., Bargueden, P., Bouty, A., Dispau, G., Donati, A., Eppelle, D., Genini, L., Guiho, P., Guihard, Q., Joubert, J.-M., Kuster, O., Médioni, D., Molinié, F., Sinanna, A., Solenne, N., Somson, S., Vieillard, L., 2015. Status of the cold test facility for the JT-60SA tokamak toroidal field coils. Fusion Eng. Des. 96–97, 208–211. https://doi.org/10.1016/j.fusengdes.2015.06.146

[2] Decool, P., Cloez, H., Jiolat, G., Tena, M., Zani, L., Hoa, C., Abdel Maksoud, W., Verrechia, M., 2016. JT-60SA TF Coils: Experimental Check of Hydraulic Operating Conditions. IEEE Trans. Appl. Supercond. 26. https://doi.org/10.1109/TASC.2016.2520585

[3] Decool, P., Maréchal, J.L., Portafaix, C., Lacroix, B., Gros, G., Verger, J.M., 2011. Detailed design studies at CEA for JT-60SA TF coils. Fusion Eng. Des. 86, 1480–1482. https://doi.org/10.1016/j.fusengdes.2010.12.028

[4] Huang, Y., 2018. Study and modelling of the thermohydraulic phenomena taking place during the quench of a superconducting magnet cooled with supercritical helium. Plasma Physics [physics.plasm-ph]. Université Paris-Saclay, 2018. English. ⟨NNT : 2018SACLS230⟩. ⟨tel-01912703⟩

[5] Lamaison, V., Hitz, D., Hoa, C., Michel, F., Reynaud, P., Roussel, P., 2010. Determination of heat loads at the interface of the JT-60SA cryogenic system. ICEC-23 809–814.

[6] Vallcorba, R., Hitz, D., Rousset, B., Lagier, B., Hoa, C., 2012. Investigations of pulsed heat loads on a forced flow supercritical helium loop: Part B: Simulation of the cryogenic circuit. Cryogenics 52, 349–361. https://doi.org/10.1016/j.cryogenics.2012.02.005

[7] Bonne, F., Hoa, C., Nicollet, S., Zani, L., Vallet, J.-C., Di Pietro, E., Wanner, M., 2019. Dynamic thermal-hydraulic simulations of the JT-60SA cryogenic system for preparing plasma operation, in: IOP Conference Series: Materials Science and Engineering. https://doi.org/10.1088/1757-899X/502/1/012129

[8] Katheder, H., 1994. Optimum thermohydraulic operation regime for cable in conduit superconductors (CICS). Cryogenics 34, 595–598. https://doi.org/https://doi.org/10.1016/S0011-2275(05)80139-0

[9] Nicollet, S., Duchateau, J.L., Fillunger, H., Martinez, A., Parodi, S., 2000. Dual channel cable in conduit thermohydraulics: Influence of some design parameters. IEEE Trans. Appl. Supercond. 10, 1102–1105. https://doi.org/10.1109/77.828425

[10] Brkić, D., 2011. Review of explicit approximations to the Colebrook relation for flow friction. Journal of Petroleum Science and Engineering 77, 34–48. https://doi.org/https://doi.org/10.1016/j.petrol.2011.02.006

[11] Bonne, F., Hoa, C., Coz, Q.L., Zani, L., Lacroix, B., Poncet, J.-M., 2019. Optimization of the cooling capacity of the cryo-magnetic system for EU DEMO at the pre-conceptual design phase. Fusion Engineering and Design. https://doi.org/https://doi.org/10.1016/j.fusengdes.2019.04.028

[12] Bonne, F., Bonnay, P., Hoa, C., Millet, F., Poncet, J-M., Rousset, B., Varin, S., Vassal, A., 2019. Simcryogenics: a Library to Simulate and Optimize Cryoplant and Cryodistribution Dynamics. IOP Conference Series: Materials Science and Engineering (MSE), Advances in Cryogenic Engineering (to be published).

[13] Nicollet, S., Abdel-Maksoud, W., Cazabonne, J., Ciazynski, D., Decool, P., Huang, Y., Lacroix, B., Torre, A., Zani, L., 2018. Parametric Analyses of JT-60SA TF Coils in the Cold Test Facility with SuperMagnet Code. IEEE Transactions on Applied Superconductivity 28. https://doi.org/10.1109/TASC.2018.2799162

[14] Nicollet, S., Ciazynski, D., Duchateau, J.L., Lacroix, B., Renard, B., 2005. Evaluation of the ITER Cable In Conduit Conductor heat transfer, in: Proceedings of the Twentieth International Cryogenic Engineering Conference, ICEC 20. pp. 589–592. https://doi.org/10.1016/B978-008044559-5/50139-3

[15] Zani, L., Barabaschi, P., Pietro, E.D., 2013. Status of European manufacture of Toroidal Field conductor and strand for JT-60SA project. Fusion Engineering and Design 88, 555–558. https://doi.org/https://doi.org/10.1016/j.fusengdes.2012.12.032

[16] Hoa, C., Bonne, F., Roussel, P., Lamaison, V., Girard, S., Fejoz, P., Goncalves, R., Vallet, J.C., Legrand, J., Fabre, Y., Pudys, V., Wanner, M., Cardella, A., Di Pietro, E., Kamiya, K., Natsume, K., Ohtsu, K., Oishi, M., Honda, A., Kashiwa, Y., Kizu, K., 2017. Performance of the JT-60SA cryogenic system under pulsed heat loads during acceptance tests, in: IOP Conference Series: Materials Science and Engineering. https://doi.org/10.1088/1757-899X/278/1/012104

[17] Kamiya, K., Natsume, K., Ohtsu, K., Oishi, M., Honda, A., Kashiwa, Y., Kizu, K., Koide, Y., Hoa, C., Michel, F., Roussel, P., Lamaison, V., Bonne, F., Dipietro, E., Cardella, A., Wanner, M., Legrand, J., Pudys, V., Langevin, B., 2017. Commissioning of the JT-60SA helium refrigerator, in: Journal of Physics: Conference Series. https://doi.org/10.1088/1742-6596/897/1/012015

[18] Davis, S., Hajnal, N., Hayakawa, A., Mayri, C., Masaki, K., Okano, F., Shibama, Y., Tomarchio, V., Tsuchiya, K., Yagyu, J., 2018. JT-60SA TF magnet assembly. Fusion Engineering and Design. https://doi.org/https://doi.org/10.1016/j.fusengdes.2018.12.070

[19] Savoldi Richard, L., Casella, F., Fiori, B., Zanino, R., 2010. The 4C code for the cryogenic circuit conductor and coil modeling in ITER. Cryogenics 50, 167–176. https://doi.org/https://doi.org/10.1016/j.cryogenics.2009.07.008

[20] Bottura, L., Rosso, C., Breschi, M., 2000. A general model for thermal, hydraulic and electric analysis of superconducting cables. Cryogenics 40, 617–626. https://doi.org/https://doi.org/10.1016/S0011-2275(01)00019-4

[21] Huang, Y., Abdel Maksoud, W., Baudouy, B., Ciazynski, D., Decool, P., Genini, L., Lacroix, B., Le Coz, Q., Nicollet, S., Nunio, F., Torre, A., Vallcorba, R., Zani, L., 2018. Numerical Modeling of the Quench

Propagation Phase in the JT-60SA TF Coils. IEEE Transactions on Applied Superconductivity 28. https://doi.org/10.1109/TASC.2018.2799176

[22] Zanino, R., Bonifetto, R., Brighenti, A., Isono, T., Ozeki, H., Savoldi, L., 2018. Prediction, experimental results and analysis of the ITER TF insert coil quench propagation tests, using the 4C code. Superconductor Science and Technology 31. https://doi.org/10.1088/1361-6668/aa9e6c

[23] Le Coz, Q., Ciazynski, D., Coleman, M., Corato, V., Lacroix, B., Nicollet, S., Nunio, F., Vallcorba, R., Zani, L., 2018. Quench Simulation of a DEMO TF Coil Using a Quasi-3D Coupling Tool. IEEE Transactions on Applied Superconductivity 28. https://doi.org/10.1109/TASC.2017.2786717

[24] Le Coz, Q., Ciazynski, D., Lacroix, B., Nicollet, S., Nunio, F., Torre, A., Vallcorba, R., Zani, L., 2017. Towards a multi-physic platform for fusion magnet design—Application to DEMO TF coil. Fusion Engineering and Design 124, 104–109. https://doi.org/10.1016/j.fusengdes.2017.03.076

[25] Bonne, F., Alamir, M., Bonnay, P., 2014. Nonlinear observer of the thermal loads applied to the helium bath of a cryogenic Joule–Thompson cycle. Journal of Process Control 24, 73–80. https://doi.org/https://doi.org/10.1016/j.jprocont.2013.12.015

[26] Froio, A., Bonifetto, R., Carli, S., Quartararo, A., Savoldi, L., Zanino, R., 2016. Design and optimization of Artificial Neural Networks for the modelling of superconducting magnets operation in tokamak fusion reactors. Journal of Computational Physics 321, 476–491. https://doi.org/https://doi.org/10.1016/j.jcp.2016.05.028